Escola de Camins
Escola Tècnica Superior d'Enginyeria de Camins, Canals i Ports
UPC BARCELONATECH

TREBALL FINAL DE MÀSTER

Computational modelling of the actin flow

Treball realitzat per:
Saskia Loosveldt Tomàs

Dirigit per:
Pablo Sáez Viñas

Màster en:
Mètodes Numèrics en Enginyeria

Barcelona, Juny 2018

Departament d'Enginyeria Civil i Ambiental

Acknowledgements

I want to acknowledge Esther Sala-Lardies and Dr. Pablo Saez for taking the time to meet with me during the development of this work.

And last, but not least, I want to thank the dearest people in my life for their unconditional support throughout all these years.

Abstract

Actin turnover plays a fundamental role in cell motility. The actin flow acts as an engine for the affective motion of motile cells by means of protrusive and retractile mechanisms conditioned also by myosin motors. Different mathematical and numerical models have appeared in literature to model the actin flow. In this work, one of the analytical models in literature will be used to include it in a finite element coupling procedure for time-dependent diffusion-convection-reaction equations governing the actin flow.

Contents

List of Figures

Chapter 1

Introduction

Cellular motility is fundamental for a large number of biological processes such as embryonic development, wound healing, immune responses and development of tissues. Cells achieve motility by performing a cycle shown in Figure 1.1 that involves: protrusion of the lamellipodium's leading edge, adhesion to the substrate, retraction of the rear and de-adhesion [3].

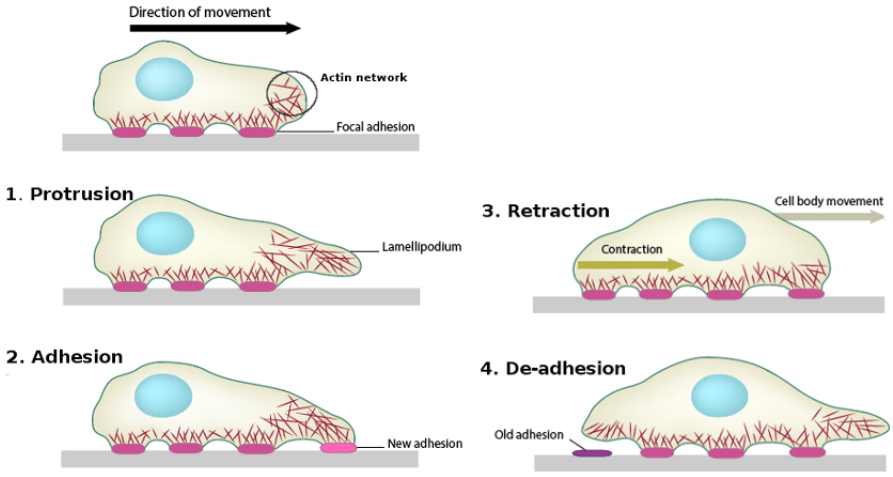

Figure 1.1: Representation of the four steps involved in cell motility. The actin network pushes the leading edge of the cell's lamellipodium, which gets adhered to the substrate. The rest of the cell's body follows the movement by retracting and then the rear part de-adheres from the substrate in order to advance. Figure adopted from [1].

This work focuses on the first step in cell locomotion. To achieve the protrusion of the leading edge a network of actin filaments pushes the leading edge forward with forces of an order of magnitude of pN. These forces allow cells to move at rates of up to $\mu m/s$.

To form the actin network, nucleation factors bind the molecular complex Arp2/3 to the side of a mother actin filament. This creates a new barbed end that elongates as actin monomers (G-actin) spontaneously polymerize into the actin filaments (F-actin) [2]. This process is represented at Figure 1.2.

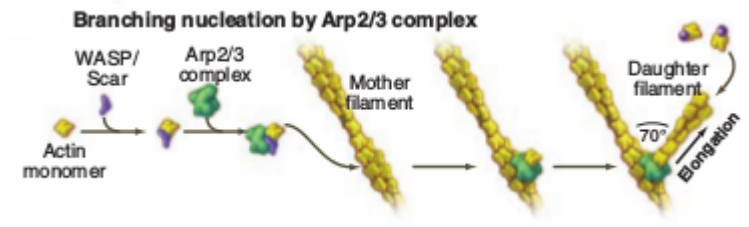

Figure 1.2: Biochemical process for which a new barbed end is created and elongated by the polymerization of actin monomers. The nucleation-promoting factor WASP binds actin monomers to the Arp2/3 complex, which then get binded to a pre-existing mother filament creating a new barbed end. The new filament elongates as new monomers polymerizes into it.Figure adopted from [2].

The elongation of the barbed end in the new filament pushes the membrane forward. The other end of the actin filament recieves the name of pointed end. The elongation of the filaments is terminated by capping proteins when they achieve lengths of about $0.5\,\mu m$. If the actin filaments were to grow longer, it is speculated that they would buckle. As the filaments age, they get severed by the protein ADF/cofilin. Therefore, the pointed ends that remain uncapped depolymerize at the rear in a tread-milling process. The dissassembly of actin filaments creates a pool of ADP actin monomers that undergo association-dissociation reactions enhanced by the protein profilin. ADP actin gets exchanged to ATP actin complexes that get recycled for subsequent polymerization [5]. This process is represented at Figure 1.3.

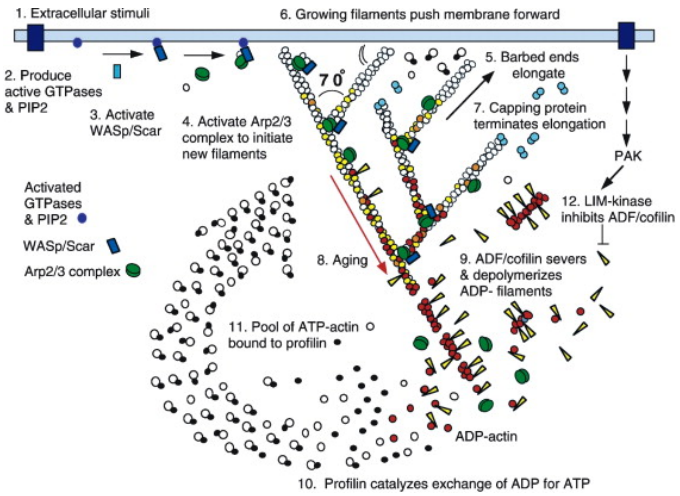

Figure 1.3: Representation of the steps involved of the polymerization and depolymerization of the actin network that regulates the protrusion of the lamellipodium. The growth of the actin network by branching pushes the membrane forward. Elongation of the network filaments is terminated at the pointed ends by capping proteins. As filaments age and get severed, they depolymerize into a pool of monomers ready to elongate the barbed ends. Figure adopted from [3].

This actin-based mechanism of motility has been observed experimentally and several models have been proposed in order to quantify it [4] [6]. Still, there are many open issues regarding the principles that govern such a complex mechanism. The combination of experimental mesurements with mathematical modelling is essential in order to characterize properly this phenomena. Furthermore, mathematical models help to rationalize and conceptualize the mechanisms, which many times are not understood experimentally.

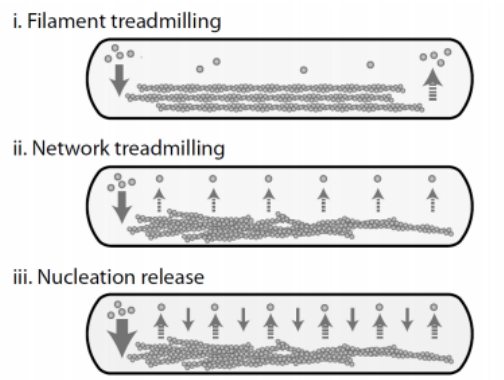

Figure 1.4: Representation of different models of actin turnover. In (i), the polymerization occurs at the barbed ends and the depolymerization occurs in the pointed ends of the filament. In (ii), the polymerization occurs at the barbed ends but the depolymerization is distributed along the lamellipodium. Finally, in (iii), both the polymerization and depolymerization occur throughout the lamellipodium. Figure adopted from [4].

In this work, a mathematical model describing the actin dynamics in a type of cell called keratocyte will be studied and discretized in order to perform numerical simulations. In Chapter 2, the theoretical model and the derivation of its analytic solution through approximations is presented. Next, in Chapter 3, the spatial and temporal discretization of the non-linear system of equations will be obtained. The results from the numerical simulations performed with the discretized system are presented in Chapter 4. Finally, the discussion and conclusions of this work will be stated in Chapter 5 and Chapter 6 respectively.

Chapter 2

Description and analysis of the theoretical model

The mathematical model was developed by Mogilner and Edelstein-Keshet [6] and describes the actin dynamics associated with cell motility through a set of partial differential equations in order to characterize the edge density of barbed ends, the concentrations for the sequestered actin complexes (G-Actin), the density of pointed (both capped and uncapped) ends, and the fluxes describing the polymerization at the barbed ends and depolymerization at the pointed ends. By introducing several approximations, the model can be solved analytically and a dependence between the protrusion velocity and the number of barbed ends pushing the membrane can be obtained.

Variables	Units	Description
B	μm^{-1}	leading edge density of uncapped barbed ends
m(x)	μm^{-2}	density of uncapped pointed ends
mc(x)	μm^{-2}	density of capped pointed ends
J_d(x)	μM s^{-1}	depolymerization flux
s(x)	μM	density of ADP-G-actin sequestered by ADF/cofilin CAD
p(x)	μM	density of ADP-G-actin-profilin PAD
β(x)	μM	density of ATP-G-actin-thymosin β4 T$_\beta$AT
a(x)	μM	density of ATP-G-actin-profilin PAT
J_p(x)	μM μm s^{-1}	Polymerization flux
V	μm s^{-1}	protrusion velocity

Table 2.1: Variables used in the model

2.1 Geometry of the model

The model simplifies the geometry of the cell lamellipodium as a 1D strip of length $L = 10\mu m$, with the leading edge located at $x = 0$.

2.2 Distribution of uncapped barbed ends

The nucleation of barbed ends along preexisting filaments as branches due to the activation of the molecular complex Arp2/3 occurs at the leading edge of the lamellipodium, in a zone with a width of hundreds of nm. Since the length scale of the lamellipodium is in terms of μm, the differential equation describing the density of barbed ends does not take into account spatial dependencies and assumes that all barbed ends are located at the leading edge:

$$\frac{dB}{dt} = n - \gamma B. \tag{2.1}$$

This differential equation describes the branching of new barbed ends in terms of the nucleation rate n and the loss of barbed ends in terms of the capping rate γ. The first approximation taken into account in order to solve the model analytically is to omit the time-dependent terms and study the system once it has reached the steady state. Therefore the steady state density of barbed ends is the following:

$$B = \frac{n}{\gamma}. \tag{2.2}$$

In this model, both the nucleation and capping rates are assumed to be constants.

2.3 Distribution and dynamics of the pointed ends

Pointed ends get described in this model in terms of those capped by Arp2/3 and those that remain free. The equation describing the dynamics of the capped ends is the following:

$$mc_t = -Vmc_x - \frac{mc}{t_1}, \tag{2.3}$$

and with the following boundary condition:

$$mc(0) = \frac{n}{V}. \tag{2.4}$$

The spatial derivative appears in order to keep the leading edge at the origin. Therefore the coordinate system of the model is moving with the edge at the protrusion velocity, since no slippage is being considered. The second term in the right hand side of (2.3) describes the uncapping of pointed ends, assumed to be a slow Poisson process characterized by the rate $1/t_1$. The boundary condition arises from assuming that capped minus ends are nucleated at the front edge with the same rate as barbed ends, meaning that the density of capped minus ends will be equal to the nucleation rate divided by the protrusion velocity.

The uncapping process leads to the creation of free pointed ends, while the complete disassembly of actin filaments, which have a lifetime characterized by the parameter t_2, causes their elimination. Thus the differential equation describing the free end density can be written as:

$$m_t = -Vm_x + \frac{mc}{t_1} - \frac{m}{t_2}, \tag{2.5}$$

with the boundary condition assuming that all minus ends at the leading origin are capped:

$$m(0) = 0. \tag{2.6}$$

Considering the steady state, the solution of (2.3) is straightforward to obtain by integrating with respect to x and applying the corresponding boundary condition:

$$mc(x) = \frac{n}{V} e^{-\frac{x}{Vt_1}}. \tag{2.7}$$

Once $mc(x)$ is known, the solution of (2.5) can also be easily computed:

$$m(x) = \frac{n}{V}\frac{t_2}{t_1}\Big[e^{-\frac{x}{Vt_1}} - e^{-\frac{x}{Vt_2}}\Big]. \tag{2.8}$$

From this distribution, two characteristic lenght scales can be defined. The first one, $l = Vt_1$, describes the average distance advanced over the time that takes for a new pointed end to be created and it has an estimaded order of magnitude of ~10 μm. The second one $\tilde{l} = Vt_2$ describes the spatial scale on which the density of F-actin decreases and is estimated to have a value of ~1 μm.

2.4 Definition of the depolymerization flux

The dissassembly of F-actin filaments regulates the recycling of actin monomers from the rear to the front of the lamellipodium. To describe this, the model defines a source of G-actin due to the dissassembly of F-actin as a flux proportional to the density of uncapped pointed ends:

$$J_d(x,t) = \frac{V_{dep}}{\delta\eta} m(x,t). \tag{2.9}$$

This specific form of the depolymerization flux is stated to be a speculation, since the details of the depolymerization phenomena are not well understood. Considering the profile of uncapped pointed ends obtained analytically in (2.8), J_d gets re-written in terms of the F-actin dissassembly rate $r = 1/t_1$, the average F-actin concentration P, and the two approximated spatial length scales l and $\tilde{l}$ discussed in the previous section:

$$J_d(x) \simeq \frac{P}{t_1}(e^{-x/l} - e^{-x/\tilde{l}}) = rP(e^{-x/l} - e^{-x/\tilde{l}}). \tag{2.10}$$

This approximation decouples the explicit dependency of $J_d(x)$ on $m(x)$. It needs to be noted that, in [6], it is not clear how (2.10) is obtained from (2.9).

2.5 Dynamics of sequestered actin complexes

In order to study the concentrations of actin monomers inside the lamellipodium, the complexes get modeled using convective terms to account for the moving coordinate system, diffusion terms to simulate the transport of the monomers along the lamellipodium and reactive terms to account for the reaction processes between monomers. Four types of complexes are considered in this model: cofilin-ADP-actin (CAD) $s(x)$, profilin-ADP-actin (PAD) $p(x)$, thymosin β4-ATP-actin (T_βAT) $\beta(x)$, and profilin-ATP-actin (PAT) $a(x)$. The differential equations for the monomer concentrations are expressed as:

$$s_t = -Vs_x + Ds_{xx} - k_1 s + k_{-1} p + J_d(x) \tag{2.11}$$

$$p_t = -Vp_x + Dp_{xx} + k_1 s - (k_{-1} + k_2) p \tag{2.12}$$

$$\beta_t = -V\beta_x + D\beta_{xx} - k_{-3}\beta + k_3 a \tag{2.13}$$

$$a_t = -Va_x + Da_{xx} + k_2 p + k_{-3}\beta - k_3 a \tag{2.14}$$

where V represents the protrusion velocity, D is the diffusion coefficient and the k-parameters are the reaction rates.

No-flux boundary conditions are considered at the front and the end of the lamellipodium for all complexes with the exception of PAT $a(x)$ complexes, since they are used up at the front edge to polymerize new actin chains:

$$\left(-D\frac{\partial a}{\partial x} + Va\right)\Big|_{x=0} = -J_p, \tag{2.15}$$

where J_p is the polymerization flux, which will be defined in Section 2.6.

As in the previous sections, to solve the equations analytically, the time dependent terms get neglected. The second approximation to solve this system is to neglect the convective terms since the protrusion velocity is estimated to be two orders of magnitude smaller than the diffusion coefficient. Therefore the system to be solved is the following:

$$Ds_{xx} - k_1 s + k_{-1} p + J_d(x) = 0 \tag{2.16}$$

$$Dp_{xx} + k_1 s - (k_{-1} + k_2)p = 0 \tag{2.17}$$

$$D\beta_{xx} - k_{-3}\beta + k_3 a = 0 \tag{2.18}$$

$$Da_{xx} + k_2 p + k_{-3}\beta - k_3 a = 0 \tag{2.19}$$

The convective term also gets neglected from the boundary condition thus:

$$\frac{da}{dx}\Big|_{x=0} = \frac{J_p}{D} \tag{2.20}$$

The last approximation comes from doing numerical simulations with (2.16), (2.17) and (2.10) that show that even though $J_d(x)$ depends on x, the results for the concentrations remain constant. Mogilner and Edelstein-Keshet do not specify how these numerical simulations were performed. With this result, the depolymerization flux gets approximated as a constant $J_d \simeq rP$.

Since the equations for the concentrations of CAD $s(x)$ and PAD $p(x)$ are not coupled with the equations for T_βAT $\beta(x)$ and PAT $a(x)$, the system to be solved analytically is the following:

$$Ds_{xx} - k_1 s + k_{-1} p + J_d = 0 \tag{2.21}$$

$$Dp_{xx} + k_1 s - (k_{-1} + k_2)p = 0 \tag{2.22}$$

Which leads to a solution were the variables are constant along x:

$$s(x) = s = \frac{k_{-1} + k_2}{k_{-1}k_2} J_d, \tag{2.23}$$

$$p(x) = p = \frac{J_d}{k_2}, \tag{2.24}$$

Substituting the result obtained in (2.24) in the second term of (2.19), the system to be solved for $\beta(x)$ and $a(x)$ can be expressed as:

$$D\beta_{xx} - k_{-3}\beta + k_3 a = 0 \tag{2.25}$$

$$Da_{xx} + J_d + k_{-3}\beta - k_3 a = 0 \tag{2.26}$$

The solution of the system without having applied boundary conditions is the following:

$$\beta(x) = \frac{c_1 + c_2 x}{k_{-3}} - \frac{k_3 J_d}{(k_3 + k_{-3})^2} - \frac{k_3 J_d x^2}{2D(k_3 + k_{-3})} - c_3 e^{\lambda x} + c_4 e^{-\lambda x}. \tag{2.27}$$

$$a(x) = \frac{c_1 + c_2 x}{k_{-3}} + \frac{k_3 J_d}{(k_3 + k_{-3})^2} - \frac{k_3 J_d x^2}{2D(k_3 + k_{-3})} + c_3 e^{\lambda x} - c_4 e^{-\lambda x}. \tag{2.28}$$

where the parameter λ is defined as:

$$\lambda = \sqrt{\frac{k_3 + k_{-3}}{D}}. \tag{2.29}$$

Applying the no flux boundary conditions and the one stated at (2.20), the coefficient c_2 has the value of:

$$c_2 = \frac{k_3 k_{-3}}{k_3 + k_{-3}} \frac{J_p}{D}. \tag{2.30}$$

From this result, another condition appears in order to make the system consistent stating that at the steady state the fluxes describing the polymerization and depolymerization of F-actin must balance:

$$J_p = J_d L. \tag{2.31}$$

Coefficients c_3 and c_4 then get determined as:

$$c_3 = 0 \text{ and} \tag{2.32}$$

$$c_4 = \frac{k_3}{k_3 + k_{-3}} \frac{J_p}{D\lambda}. \tag{2.33}$$

The fact that the total amount of actin is equal to the amount of F-actin plus the amount of G-actin is the last condition needed in order to obtain the parameter c_1. Recalling the approximation of $J_d \simeq rP$ and using (2.31), the total amount of G-actin can be written as:

$$A = P + [G] = \frac{J_p}{rL} + [G] \rightarrow [G] = (\bar{a} + \bar{\beta} + s + p) = A - \frac{J_p}{rL}. \tag{2.34}$$

where s and p are the concentrations obtained in (2.23) and (2.24), and $\bar{a} + \bar{\beta}$ is the average amount of PAT and T_βAT complexes $a(x) + b(x)$ integrated over the lamellipodium:

$$\bar{a} + \bar{\beta} \equiv \frac{1}{L} \int_0^L (a(x) + b(x))dx = c_1 \frac{k_3 + k_{-3}}{k_3 k_{-3}} + \frac{J_p L}{3D}. \tag{2.35}$$

Substituting (2.35) in (2.34), the coefficient c_1 gets expressed as:

$$c_1 = \frac{k_3 k_{-3}}{k_3 + k_{-3}} \left(A - (\tau_{dep} + \tau_{cof} + \tau_{dif}) \frac{J_p}{L} \right). \tag{2.36}$$

In which the τ coefficients are expressed in terms of the model parameters:

$$\tau_{dep} = \frac{1}{r}, \ \tau_{cof} = \frac{k_1 + k_{-1} + k_2}{k_1 k_2}, \ \tau_{dif} = \frac{L^2}{3D}. \tag{2.37}$$

With all the approximations and assumptions mentioned, an analytic dependency of the monomer concentrations in space is found in terms of the depolymerization flux J_d (taken as a constant), and the variables V and J_p which are yet to be defined.

2.6 Definition of the polymerization flux

At the leading edge, the available concentration of PAT $a(x)$ monomers regulates the polymerization of actin filaments. Thus, the flux created by these complexes is defined as the polymerization flux J_p, used as a boundary condition in the previous section. The magnitude of this flux is defined in the model as:

$$J_p = \frac{VB}{\delta\eta}, \tag{2.38}$$

in which the term V/δ represents the rate of monomer addition per filament and the term $1/\eta$ is used as a conversion factor from concentration units μM to number of monomers per μm^2 .

2.7 Derivation of the protrusion velocity

Once the dependance of the variables of model in x has been found, the last step is to obtain the profile of the protrusion velocity. The model starts by defining a free polymerization velocity in terms of the polymerization rate constant k_{on} and the concentration of PAT available on the leading edge $a(x = 0)$:

$$V_0 = k_{on}\delta a(x = 0). \tag{2.39}$$

The actual protrusion velocity needs to be written in terms of V_0 and in terms of a resistance force per unit of length at the leading edge F. The expression relating these variables is formulated from previous theoretical work, since there were no experimental measurements available at the time this theoretical model was developed:

$$V = V_0 exp\left(\frac{-F\delta}{k_B T B}\right). \tag{2.40}$$

This expression considers the protrusion velocity to be the free polymerization velocity weighted by a Boltzmann factor in which the exponent represents the work done against the membrane by a population of filaments B in units of thermal energy.

To obtain the final $V(F, B)$ dependency, the concentration profile of PAT $a(x)$ obtained in (2.28) gets evaluated at $x = 0$ and the boundary condition in (2.38) gets applied, thus:

$$a(x = 0) = \frac{k_{-3}}{k_3 + k_{-3}}\left(A - \frac{J_p\tau}{L}\right) = \frac{k_{-3}}{k_3 + k_{-3}}\left(A - \frac{VB\tau}{\delta\eta L}\right), \tag{2.41}$$

where τ depends on the coefficients defined in (2.37) and a further parameter τ_{thy}:

$$\tau = \tau_{dep} + \tau_{cof} + \tau_{dif} + \tau_{thy}, \tag{2.42}$$

$$\tau_{thy} = \frac{k_3}{k_{-3}(k_3 + k_{-3})}\left[\sqrt{\frac{L^2(k_3 + k_{-3})}{D}} - 1\right]. \tag{2.43}$$

Combining expressions (2.39) and (2.41) with (2.40), the model yields to the equation linking the protrusion velocity with the number of barbed ends:

$$V = \frac{\bar{V}}{\kappa\exp(\mathrm{w/B}) + \alpha B}, \tag{2.44}$$

where:

$$\bar{V} = k_{on}\delta A,\ \kappa = \left(1 + \frac{k_3}{k_{-3}}\right),\ w = \frac{F\delta}{k_B T},\ \alpha = \left(\frac{k_{on}\tau}{\eta L}\right) \text{and } B = \frac{n}{\gamma} \tag{2.45}$$

2.8 Implications from the theoretical model

Several conclusion can be drawn from the analytic expressions obtained by solving the system through approximations. The value of the parameters used to plot the analytic expressions are stated at Table 2.2.

Parameters	Values	Description
n	~100 μm^{-1}s^{-1}	Nucleation rate
γ	~1 s^{-1}	Barbed end capping rate (c)
t_1	~30 s	Average time of uncapping of minus ends
t_2	~1 s	Average filament lifetime
V_{dep}	~0.1 μm s^{-1}	Effective rate of depolymerization
δ	2.2 nm	Filament length increment per monomer
η	100 μM^{-1} μm^{-2}	Conversion factor to units of concentration
$r=1/t_1$	~1/30 s^{-1}	F-actin dissassembly rate
P	~200 μM	Average F-actin concentration
l	~10 μm	Defined in Section 2.3
$\tilde{l}$	~1 μm	Defined in Section 2.3
A	~250 μM	Total actin concentration
P	~200 μM	Average F-actin concentration
L	≃10 μm	Length of the lamellipodium
D	30 μm^{2}s^{-1}	Diffusion coefficent of G-actin complexes
k_1	2 s^{-1}	CAD → PAD reaction rate
k_{-1}	10 s^{-1}	PAD → CAD reaction rate
k_2	20 s^{-1}	PAD → PAT reaction rate
k_3	2 s^{-1}	PAT → T$_\beta$AT reaction rate
k_{-3}	2 s^{-1}	T$_\beta$AT → PAT reaction rate

Table 2.2: Variables and parameters used in the model

Regarding the F-actin variables, the density of barbed ends B pushing the membrane is found to be a constant depending on the nucleation rate n and the capping rate at the leading edge γ. The density for this type of cells is estimated to have a value of $B \sim 50 - 250\,\mu m^{-1}$. On the other hand, the density of the pointed ends, both capped and uncapped, has a dependency on x as shown in Figure 2.1.

The model predicts an exponential decay of capped ends $mc(x)$ from the front to the the rear of the lamellipodium, starting from the value at $x = 0$ given by the boundary condition in (2.4). For the pointed ends that remain uncapped, the density increases exponentially away from the leading edge up until a certain distance and then decays exponentially toward the end. It can be noted that the density of capped ends is an order of magnitude greater than the ends that remain uncapped.

For the G-actin monomers, Figure 2.2 shows how the stationary concentrations for $s(x)$ and $p(x)$ are constants, whereas the concentration for $\beta(x)$ and $a(x)$ decrease from the rear to the front of the lamellipodium. This concentration gradient indicates that in the leading edge, the monomers are being used to extend the length of the F-actin chains by polymerizing into them.

It needs to be stated that in [6], the plots for variables $\beta(x)$ and $a(x)$ do not showcase the same behaviour that is presented in Figure 2.2. Still, in Section 4.1 it will be shown how the numerical simulations lead to the behaviour shown in Figure 2.2. Therefore, it remains unclear how these variables are being plotted in [6].

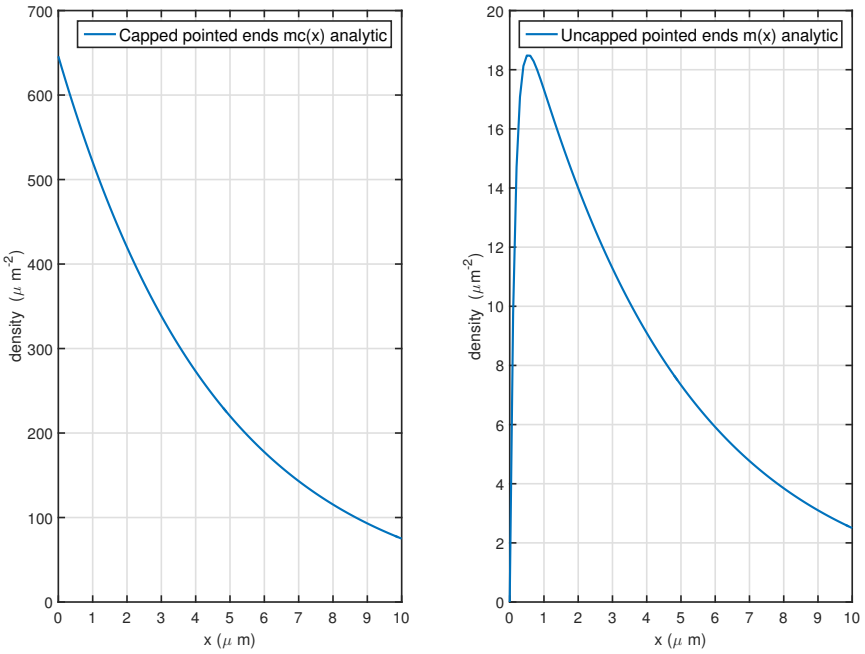

Figure 2.1: Analytic densities along the lamellipodiumium of the pointed ends, both capped and uncapped, for $B = 100\,\mu m^{-1}$, $F = 100\,p\mathrm{N}/\mu m$ and $J_d = 7\,\mu M s^{-1}$.

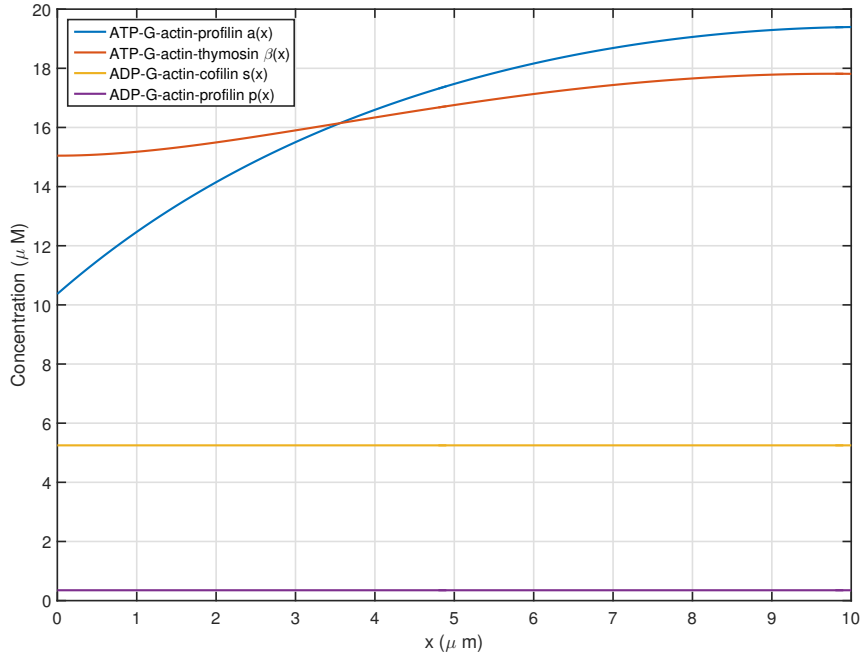

Figure 2.2: Analytic concentrations along the lamellipodiumium of the G-actin monomers for $B = 100\,\mu m^{-1}$, $F = 100\,p\mathrm{N}/\mu m$ and $J_d = 7\,\mu M s^{-1}$.

The dependency of the protrusion velocity on the number of barbed ends predicts an optimal value of B for which the cell achieves a maximum velocity for a given value of the protrusion resistance force. For a number of barbed ends smaller than the optimal value, the velocity drops dramatically. Whereas, for a number of barbed ends greater than the optimal value, the velocity also drops but at a lower rate. This result can be appreciated in Figure 2.3. Furthermore, it can be appreciated how the protrusion velocity is inversely proportional to the resistance force.

Again, some discrepancies have been found between Figure 2.3 and the figure where this dependency is presented in [6]. Although the dependency is the same in both plots, the maximum values for the velocity shown in Figure 2.3 are slightly larger than the values presented in [6]. For instance, in [6] the maximum for $F = 50pN/\mu m$ appears to be at $V \simeq 0.39\mu m/s$, whereas in Figure 2.3 the maximum is found to be at $V \simeq 0.42\mu m/s$. The source of this differences also remains unclear, since the values for the parameters that are being used to plot the expressions in the present work are the same that are stated in [6].

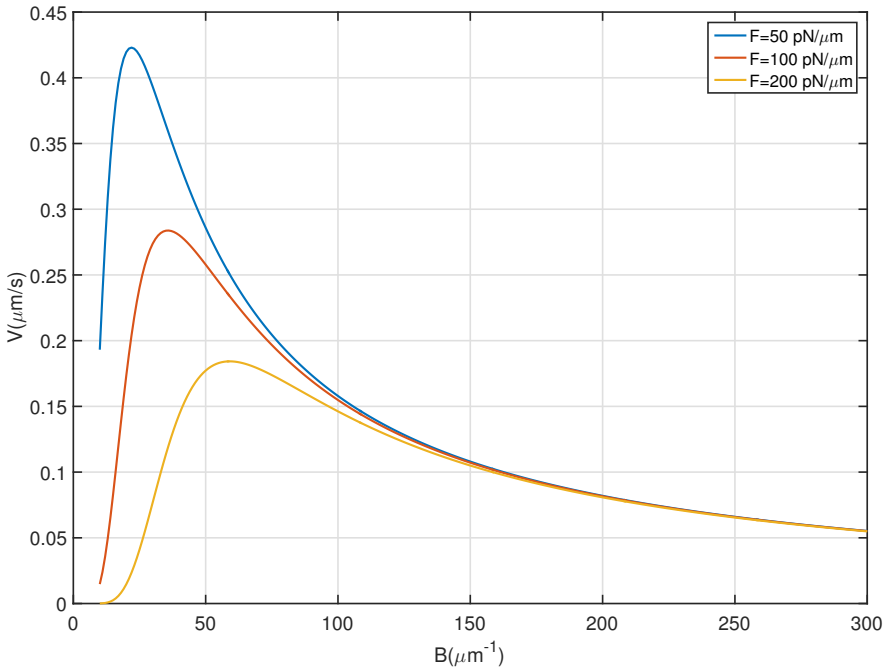

Figure 2.3: Analytic dependency of the protrusion velocity on the number of barbed end B and the resistance force F.

Chapter 3

Finite element formulation of the model

Once the theoretical model has been proposed and an analytical solution has been obtained through approximations and assumptions, the aim of this work is to discretize the coupled nonlinear system of equations to solve it numerically without having to use simplifications.

3.1 Strong form

Defining the spacial domain as the lenght of the lamellipod $\Omega \equiv [0, L]$, the strong form of the problem is:

$$
\begin{aligned}
&B_t = n - \gamma B && \text{in }]0,\mathrm{T}[, \\
&mc_t = -V mc_x - \frac{mc}{t_1} && \text{in } \Omega \times]0,\mathrm{T}[, \\
&m_t = -V m_x + \frac{mc}{t_1} - \frac{m}{t_2} && \text{in } \Omega \times]0,\mathrm{T}[, \\
&s_t = -V s_x + D s_{xx} - k_1 s + k_{-1} p + \frac{V_{dep}}{\delta \eta} m && \text{in } \Omega \times]0,\mathrm{T}[, \\
&p_t = -V p_x + D p_{xx} + k_1 s - (k_{-1} + k_2) p && \text{in } \Omega \times]0,\mathrm{T}[, \\
&\beta_t = -V \beta_x + D \beta_{xx} - k_{-3} \beta + k_3 a && \text{in } \Omega \times]0,\mathrm{T}[, \\
&a_t = -V a_x + D a_{xx} + k_2 p + k_{-3} \beta - k_3 a && \text{in } \Omega \times]0,\mathrm{T}[,
\end{aligned}
\tag{3.1}
$$

with boundary conditions:

$$
\begin{aligned}
mc &= \frac{n}{V} && \text{on } \Gamma_D \times]0,\mathrm{T}[, \\
m &= 0 && \text{on } \Gamma_D \times]0,\mathrm{T}[, \\
s_n &= p_n = \beta_n = 0 && \text{on } \Gamma_N \times]0,\mathrm{T}[, \\
-D\frac{\partial a}{\partial x} &+ Va = -J_p && \text{on } \Gamma_R \times]0,\mathrm{T}[,
\end{aligned} \tag{3.2}
$$

where the Dirichlet domain is set at the leading edge $\Gamma_D = \{0\}$ for the F-actin variables, the Neumann domain is set at $\Gamma_N = \{0, L\}$ for the G-actin variables s, p, β, and the Robin domain is set at $\Gamma_R = \{0\}$ for the G-actin variable a. The initial conditions are set arbitrarily.

3.2 Weak form

The weak form of the problem is obtained in terms of test and trial function spaces, $\mathcal{V}$ and $\mathcal{S}_t$ which get defined over the Sobolev space $\mathcal{H}^1$ to ensure square integrable functions and derivatives [7].

The functions in $\mathcal{V}$ satisfy homogeneous boundary conditions on Γ_D and do not depend on time:

$$
\mathcal{V} \equiv \{w \in \mathcal{H}^1(\Omega) \mid w = 0 \text{ on } \Gamma_D\}. \tag{3.3}
$$

On the other hand, the functions in $\mathcal{S}_t$ need take into account the time dependency of the approximate solution and need to verify the Dirichlet boundary conditions:

$$
\mathcal{S}_t \equiv \{u \mid u(\cdot, t) \in \mathcal{H}^1(\Omega),\ t \in [0, T] \text{ and } u(x, t) = u_D \text{ for x} \in \Gamma_D\}. \tag{3.4}
$$

Thus, the weak form of the problem defined in Section 3.1 will have variables $mc(x,t)$, $m(x,t)$, $s(x,t)$, $p(x,t)$, $\beta(x,t)$, $a(x,t) \in \mathcal{S}_t$ such that $\forall\, w \in \mathcal{V}$:

$$
\begin{aligned}
B_t &= n - \gamma B \\
(w, mc_t) &= -c(V; w, mc) - (w, \frac{1}{t_1} mc) \\
(w, m_t) &= -c(V; w, m) + (w, \frac{1}{t_1} mc) - (w, \frac{1}{t_2} m) \\
(w, s_t) &= -c(V; w, s) - a(w, s) - (w, k_1 s) + (w, k_{-1} p) + (w, \frac{V_{dep}}{\delta \eta} m) \\
(w, p_t) &= -c(V; w, p) - a(w, p) + (w, k_1 s) - (w, (k_{-1} + k_2) p) \\
(w, \beta_t) &= -c(V; w, \beta) - a(w, \beta) - (w, k_{-3} \beta) + (w, k_3 a) \\
(w, a_t) &= -c(V; w, a) - a(w, a) + (w, k_2 p) + (w, k_{-3} \beta) - (w, k_3 a) - (w, Va + J_p)_{\Gamma_R},
\end{aligned}
\tag{3.5}
$$

where the second order terms have been reduced to first order terms by integrating by parts and applying the divergence theorem. The notation used for the integral forms stands for:

$$
\begin{aligned}
(w, u) &= \int_0^L wu \, dx, & (w, Va + J_p)_{\Gamma_R} &= w(\Gamma_R)[Va(\Gamma_R) + J_p] \\
c(V; w, u) &= \int_0^L w \, V \, \frac{du}{dx} dx, & a(w, u) &= \int_0^L \frac{dw}{dx} D \frac{du}{dx} \, dx,
\end{aligned}
$$

in which u is any variable that can be multiplied by a constant.

3.3 Spatial discretization

Once the weak form of the problem has been obtained, the domain gets discretized in a finite element mesh with a set of nodes η, where η_D is the subset of nodes belonging to the Dirichlet boundary. The semi-discrete Galerkin formulation of the problem is obtained by restricting $\mathcal{S}$ and $\mathcal{V}$ to the finite dimensional spaces $\mathcal{S}^h$ and $\mathcal{V}^h$. Then, the trial solution can be written in terms of a shape function N_A associated to a node A in the finite element mesh and the nodal unknown $u_A(t)$:

$$
u^h(x, t) = \sum_{A \in \eta \setminus \eta_D} N_A(x) u_A(t) + \sum_{A \in \eta_D} N_A(x) u_D(x_A, t). \tag{3.6}
$$

In the Galerkin formulation the test functions w^h get defined as:

$$
w^h \in \mathcal{V}^h \equiv \operatorname*{span}_{A \in \eta \setminus \eta_A} \{N_A\}. \tag{3.7}
$$

The assembly of each element contribution to the discrete weak form into the complete system allows to write the weak form in terms of a matrix equation:

$$
\begin{aligned}
& B_t = n - \gamma B \\
& \mathbf{M}\,\dot{\mathbf{mc}} + (\mathbf{C} + \frac{1}{t_1}\mathbf{M})\,\mathbf{m_c} = -\sum_{b=1}^{n_{en}} (\, c(V; N_a, N_b)_{\Omega_e} + \frac{1}{t_1}(N_a, N_b)_{\Omega^e})\frac{n}{V} \\
& \mathbf{M}\,\dot{\mathbf{m}} + (\mathbf{C} + \frac{1}{t_2}\mathbf{M})\,\mathbf{m} - \frac{1}{t_1}\mathbf{M}\,\mathbf{m_c} = \mathbf{0} \\
& \mathbf{M}\,\dot{\mathbf{s}} + (\mathbf{C} + \mathbf{K} + k_1\mathbf{M})\,\mathbf{s} - k_{-1}\mathbf{M}\,\mathbf{p} - \frac{V_{dep}}{\delta\eta}\mathbf{M}\,\mathbf{m} = \mathbf{0} \\
& \mathbf{M}\,\dot{\mathbf{p}} + (\mathbf{C} + \mathbf{K} + (k_{-1} + k_2)\mathbf{M})\,\mathbf{p} - k_1\mathbf{M}\,\mathbf{s} = \mathbf{0} \\
& \mathbf{M}\,\dot{\boldsymbol{\beta}} + (\mathbf{C} + \mathbf{K} + k_{-3}\mathbf{M})\,\boldsymbol{\beta} - k_3\mathbf{M}\,\mathbf{a} = \mathbf{0} \\
& \mathbf{M}\,\dot{\mathbf{a}} + (\mathbf{C} + \mathbf{K} + k_3\mathbf{M})\,\mathbf{a} - k_2\mathbf{M}\,\mathbf{p} - k_{-3}\mathbf{M}\,\boldsymbol{\beta} = -(N_a, Va + J_p)_{\partial\Omega^e \cap \Gamma_R}.
\end{aligned}
\tag{3.8}
$$

The vectors representing each variable contain the nodal values of said variable and its time derivative. The matrices $\mathbf{C}$, $\mathbf{K}$, $\mathbf{M}$ represent the convection, stiffness and mass matrix respectively, and are defined as the topological assembly $\mathbf{A}^e$ of element contributions of length l^e as follows:

$$
\mathbf{C} \equiv \mathbf{A}^e \int_{l^e} N_a V \frac{dN_b}{dx} dl \qquad \mathbf{K} \equiv \mathbf{A}^e \int_{l^e} \frac{dN_a}{dx} D \frac{dN_b}{dx} dl \qquad \mathbf{M} \equiv \mathbf{A}^e \int_{l^e} N_a N_b dl. \tag{3.9}
$$

The previous expressions stand for a semi-discrete Galerkin scheme, since the temporal discretization has still to be performed.

3.4 Temporal discretization

Commonly used methods to discretize in time are the θ family of methods, which compute the unknown u^{n+1} at time t^{n+1} from the value of u^n at time t^n. Solving for the incremental unknown $\Delta u = u^{n+1} - u^n$, the θ scheme can be written as:

$$
(w, \frac{\Delta u}{\Delta t}) - \theta(w, \Delta u_t) = (w, u_t^n) \tag{3.10}
$$

This scheme is applied to the weak form of the system, where the time derivatives are substituted by the expressions in (3.6). The value of the θ parameter determines the properties of the scheme. The θ-method that has been implemented to discretize the temporal derivatives is Forward Euler, which implies that $\theta = 0$. This leads to a conditionally stable scheme that decouples the whole system.

Implementing the temporal discretization in (3.10) with $\theta = 0$ to the space discretized system in (3.9), at each time step the equations to be solved will be:

$$
\begin{aligned}
B^{n+1} &= B^n + dt(n - \gamma B^n) \\
\frac{\mathbf{M}}{dt}\Delta mc &= -(\mathbf{C} + \frac{\mathbf{M}}{t_1})mc^n \\
\frac{\mathbf{M}}{dt}\Delta m &= -(\mathbf{C} + \frac{\mathbf{M}}{t_2})m^n + \frac{\mathbf{M}}{t_1}mc^n \\
\frac{\mathbf{M}}{dt}\Delta s &= -(\mathbf{C} + \mathbf{K} + k_1\mathbf{M})s^n + k_{-1}\mathbf{M}p^n + \frac{V_{dep}}{\delta\eta}\mathbf{M}m^n \\
\frac{\mathbf{M}}{dt}\Delta p &= -(\mathbf{C} + \mathbf{K} + (k_{-1} + k_2)\mathbf{M})p^n + k_1\mathbf{M}s^n \\
\frac{\mathbf{M}}{dt}\Delta \beta &= -(\mathbf{C} + \mathbf{K} + k_{-3}\mathbf{M})\beta^n + k_3\mathbf{M}a^n \\
\frac{\mathbf{M}}{dt}\Delta a &= -(\mathbf{C} + \mathbf{K} + k_3\mathbf{M})a^n + k_{-3}\mathbf{M}\beta^n + k_2\mathbf{M}p^n,
\end{aligned}
\tag{3.11}
$$

where the boundary conditions will be applied at the corresponding nodes. The initial conditions have been set arbitrarily, since the system should converge to a steady state.

3.5 Linearization

As stated in (2.39) and (2.40), the protrusion velocity depends on the concentration of PAT $a(x,t)$ at the front of the lamellipodium, thus making the system non-linear. In order to compute the solution, the system has been linearized using a fixed point iteration, defined by the following algorithm:

Algorithm 1 Fixed point algorithm

1: Set a tolerance ϵ and a maximum number of iterations k
2: Set an initial guess for the vector of unknowns $\xi^0 = [mc^0\ m^0\ s^0\ p^0\ \beta^0\ a^0]^T$
3: Compute V^0 with the concentration a^0
4: **while** $||\xi^k - \xi^{k-1} < \epsilon||$ **do**
5: Solve the linear system in (3.9) as $A(\xi^{k-1})\xi^k = b$
6: Compute V^k with the result a^k
7: Update the variables
8: **end while**

Chapter 4

Numerical simulations

Several numerical cases have been run in order to study the F-actin density, G-actin concentrations and velocity of fast moving cells. To compute the numerical simulations, the 1D domain representing the lamellipodium gets discretized using 100 linear elements, that is two-noded elements. The quadrature used to compute the integrals numerically is a two-point Gauss quadrature.

4.1 Steady case with a constant depolymerization flux J_d

The analytic solution for the steady case obtained through the approximations discussed in Chapter 2, can be used as a way to test the code in order to ensure that the discretization and linearization of the system have been implemented properly. Therefore, the first numerical simulation that was run considers the system in which the time dependant and convective terms have been neglected and J_d is taken as a constant. While this is a system that has an analytic solution, solving it numerically is not possible because the matrix arising from the discretization is singular. This issue appears because the only variables in which Dirichlet boundary conditions are being applied are $mc(x)$ and $m(x)$. Recalling the approximations in Chapter 2, the equations for the F-actin variables, $mc(x)$ and $m(x)$, get decoupled from the equations for the G-actin variables $s(x)$, $p(x)$, $\beta(x)$ and $a(x)$. Furthermore, the Robin boundary condition for $a(x = 0)$ in (2.15) gets approximated to a Neumann boundary condition as in (2.20), while no-flux Neumann boundary conditions get applied for variables $s(x)$, $p(x)$, $\beta(x)$. Therefore, the coupled system for the G-actin variables lacks a Dirichlet condition to avoid singularities in the discretization.

Due to this issue, the system for the steady case with J_d taken as a constant needs to include the convective terms to ensure that the Robin boundary condition gets applied to make the system non-singular. Figure 4.1 and Figure 4.2 show the results for the density of the F-actin variables and concentration of the G-actin monomers in the lamellipodium for a number of barbed ends $B = 100\,\mu m^{-1}$ and a resistance force $F = 100\,p\mathrm{N}/\mu m$. The value for the velocity obtained by the numerical simulations is shown in Table 4.1.

For the capped ends, the exponential decay from the front to the rear of the lamellipodium is clearly showcased. For the uncapped ends, the exponential increase of the density and then subsequent exponential decrease is also obtained. As for the G-actin variables, on one hand, the numerically obtained concentrations for $s(x)$ and $p(x)$ remain constant along x and have the same value that is predicted by the analytic model. On the other hand, the concentrations computed for $\beta(x)$ and $a(x)$ showcase the same gradient from the rear to the front as expected by the analytic model, but the values achieved are larger than expected. Regarding the protrusion velocity, the value obtained by the numerical simulation presents a larger value with a 10% difference compared to the expected analytic value.

Although the analytic and numerically obtained dependencies exhibit a similar behaviour, they present differences in their values for the variables $mc(x)$, $m(x)$, $\beta(x)$ and $a(x)$. This differences can be explained in terms of the protrusion velocity. First, the system that is being solved numerically is not the same that is being solved analytically due to the inclusion of convective terms that depend on the protrusion velocity. This convective terms affect both the system equations and the boundary conditions for $a(x)$. Furthermore, the computed protrusion velocity is larger than expected, and since the system is coupled this discrepancy ends up affecting other variables. An explanation for these differences will be presented in Section 4.4.

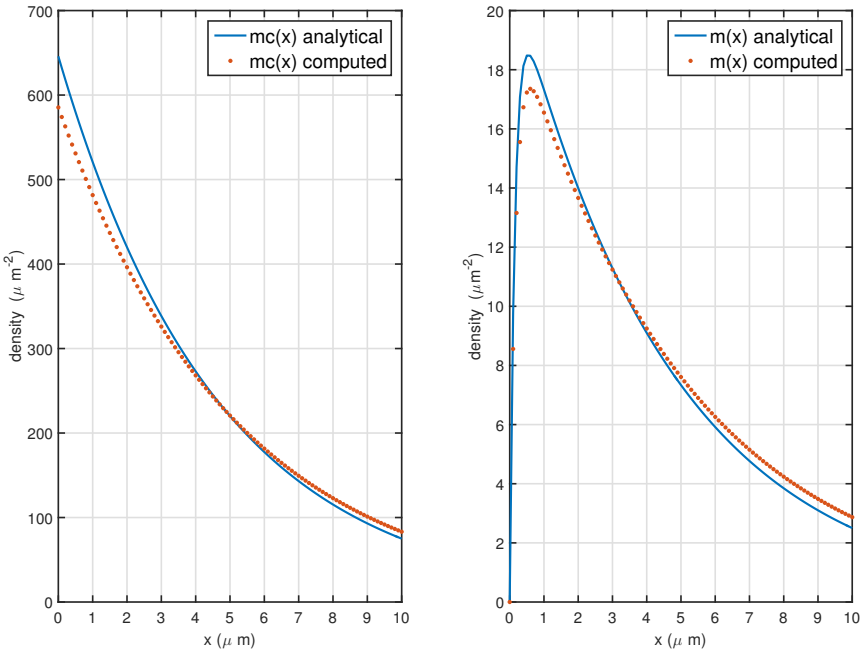

Figure 4.1: Computed densities along the lamellipodium of the pointed ends, both capped and uncapped, compared to the analytic expressions derived from the model for $B = 100\,\mu m^{-1}$, $F = 100\,p\mathrm{N}/\mu m$ and $J_d = 7\,\mu M s^{-1}$.

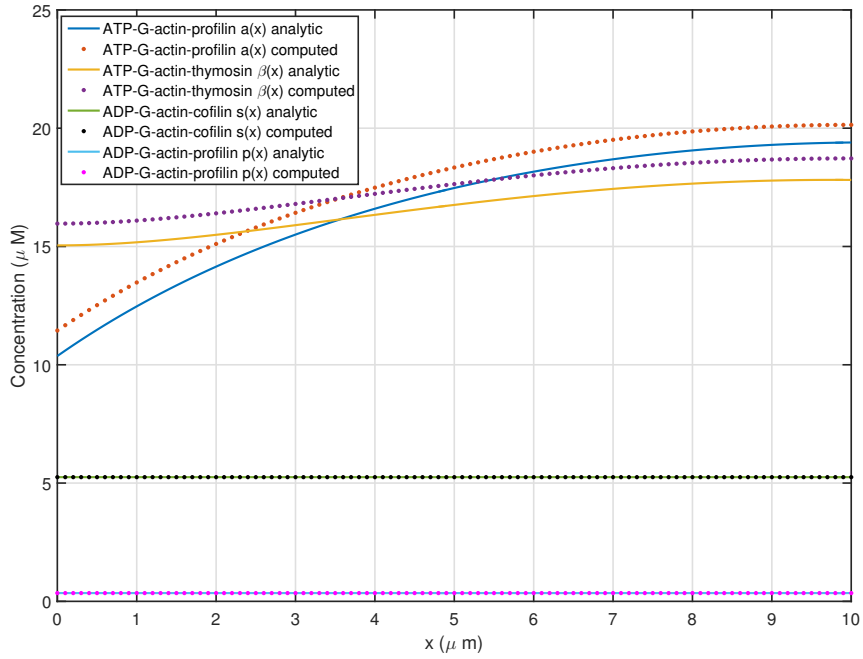

Figure 4.2: Computed concentrations along the lamellipodium of the G-actin monomers compared to the analytic expressions derived from the model for $B = 100\,\mu m^{-1}$, $F = 100\,p\mathrm{N}/\mu m$ and $J_d = 7\,\mu M s^{-1}$.

	Computed	Analytic
Front velocity V (μm/s)	0.1708	0.1548

Table 4.1: Computed front velocity compared to the expected analytic value for $B = 100\,\mu m^{-1}$, $F = 100\,p$N and $J_d = 7\,\mu M s^{-1}$.

To study the $V(F, B)$ dependency, the code has been used to solve the system for several values of B. Figure 4.3 shows the dependency obtained with the simulations. Unlike the densities and concentrations computed for the case in which $B = 100\,\mu m^{-1}$ and $F = 100\,p$N, the dependency obtained by the numerical simulation is not the one that is expected by the analytic results. The numerical results show how the velocity increases with the number of barbed ends, Instead of showing an optimal value of B for which the velocity is maximum. The rate at which the velocity increases gets diminished as the number of barbed ends grows. While this result appears to be unexpected, it has been found that it can be explained in terms of the analytic model. The discussion will be presented in sections 4.4 and 4.5.

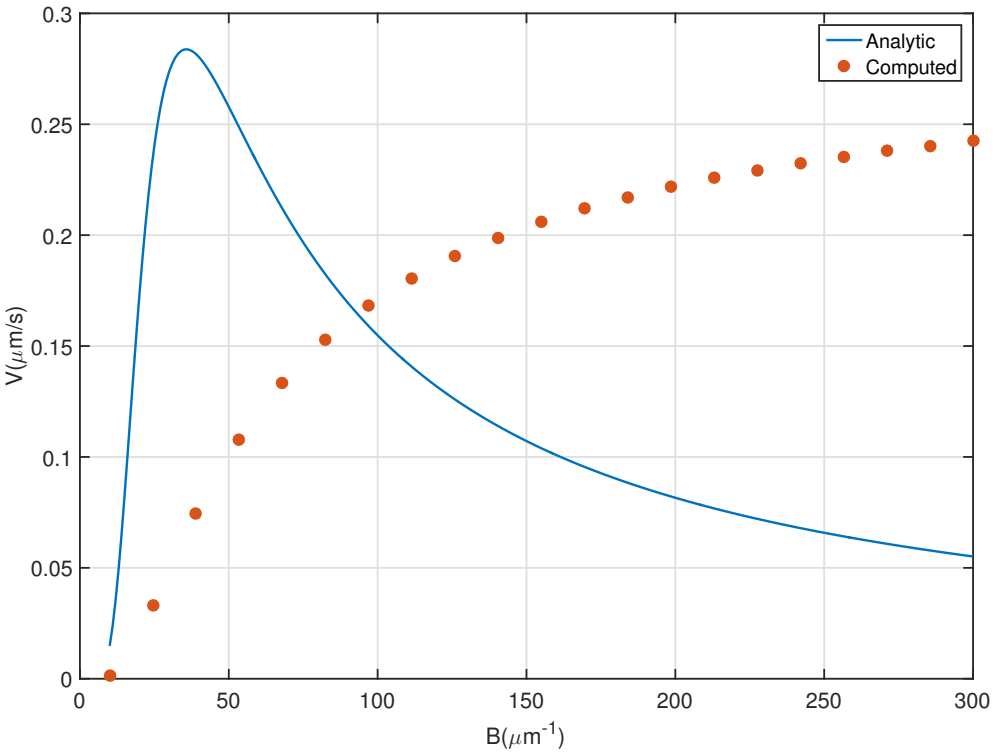

Figure 4.3: Comparison between the computed and analytic protusion velocity with respect to the number of barbed ends for $F = 100\,p\text{N}/\mu m^{-1}$.

4.2 Steady case with a depolymerization flux $J_d = J_d(m(x))$

Considering the results in Section 4.1, the simulations for the current section have been computed just for $B = 100\,\mu m^{-1}$, which is a value for B where the numerical results showed similarities with the analytic results. Recalling the definition of the depolymerization flux:

$$J_d(x,t) = \frac{V_{dep}}{\delta\eta} m(x,t). \tag{4.1}$$

With this definition, now the system to be solved couples the F-actin variable $m(x)$ to the G-actin monomer $s(x)$. This is a system that has not been solved analytically in [6]. Still, as a reference, the numerical results will be compared to the analytic solution presented in Chapter 2 for a constant depolymerization flux. The numerical results for this case are not expected to be exactly as the analytic results predict because the definition of the depolymerization flux is different. Still, the order of magnitude and behaviour of the variables should bare some similarities in both cases since the equations are describing the same physical system.

The numerical results for the F-actin densities and G-actin concentrations are shown in Figure 4.4 and Figure 4.5 respectively, and the computed value for the protrusion velocity is stated in Table 4.2.

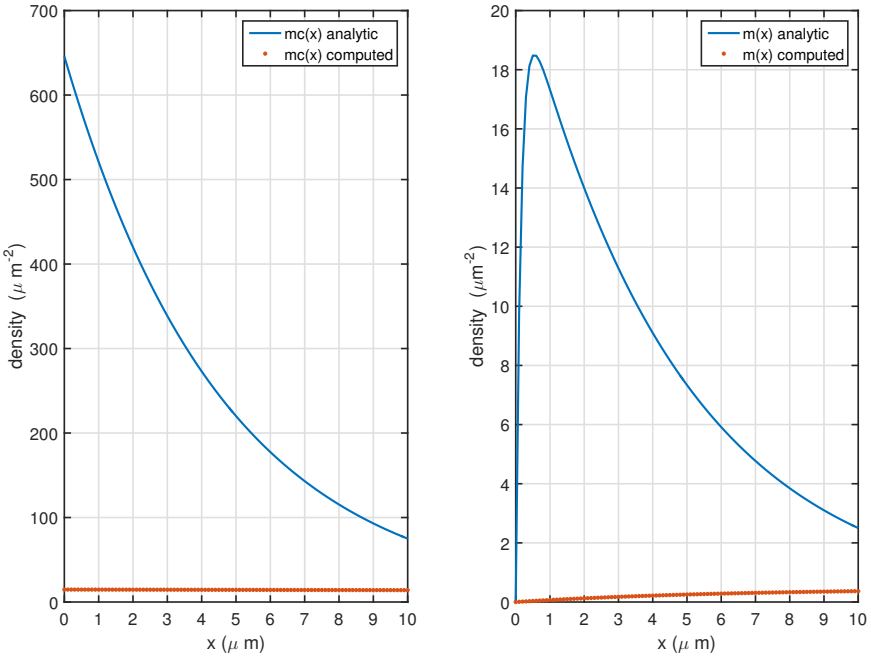

Figure 4.4: Computed densities along the lamellipodium of the pointed ends, both capped and uncapped, compared to the analytic expressions derived from the model for $B = 100\,\mu m^{-1}$, $F = 100\,p\mathrm{N}/\mu m$ and $J_d = \frac{V_{dep}}{\delta\eta} m(x,t)$.

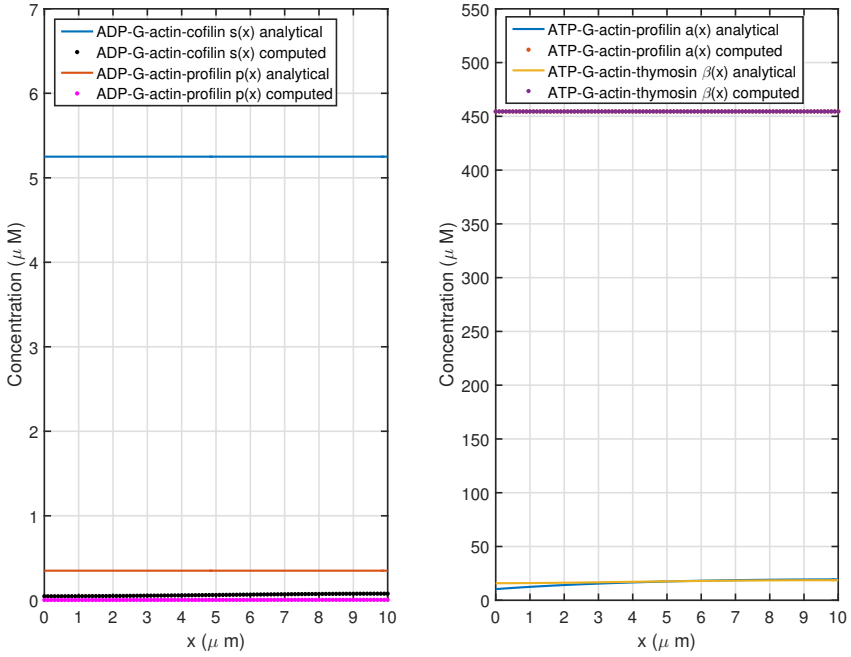

Figure 4.5: Computed concentrations along the lamellipodium of the G-actin monomers compared to the analytic expressions derived from the model for $B = 100\,\mu m^{-1}$, $F = 100\,p\mathrm{N}/\mu m$ and $J_d = \frac{V_{dep}}{\delta\eta} m(x,t)$.

	Computed	Analytic
Front velocity V (μm/s)	6.7823	0.1548

Table 4.2: Computed front velocity compared to the expected analytic value for $B = 100\,\mu m^{-1}$, $F = 100\,p$N and $J_d = \frac{V_{dep}}{\delta\eta} m(x,t)$.

The numerical results are showcasing a big discrepancy in both the order of magnitude and dependency that are expected for each variable.

For the density of capped ends, the computed values are two orders of magnitude smaller than expected and the exponential decay form the from the front to the rear cannot be appreciated. Likewise, the density for the pointed ends obtained numerically is also two orders of magnitude smaller than expected and appears to be increasing from the front to the rear of the lamellipodium. This results contradicts the several implications from the model. The first one states that the density of capped ends should be two orders of magnitude larger than the density of pointed ends. The second one states that the density of capped ends shows and exponential decrease from the front to the rear of the lamellipodium. And the third one that describes the density of uncapped ends as having an exponential increase away from the leading edge up to a certain distance, and then presents an exponential decay towards the end.

Regarding the monomer concentrations, the numerical results are also contradicting the implications from the model. While it is true that the computed concentrations for $s(x)$ and $p(x)$ remain constant along the lamellipodium, their values are close to zero, which is not what the analytic model predicts. On the other hand, the concentrations for $\beta(x)$ and $a(x)$ do not show any gradient from the rear to the front of the lamellipodium and their dependencies overlap reaching concentration values two orders of magnitude higher than expected.

As for the protrusion velocity, the computed result presents a 40% error leading to a value that is one order of magnitude larger than expected.

This results seem to indicate that the definition of the depolymerization flux used in this section may be an issue. A further discussion regarding the fluxes will be presented in Section 4.5.

4.3 Unsteady case

To finish the numerical simulations, the time dependant terms have been included so that the discretized problem obtained in (3.9) is solved, thus solving the equations from the model without imposing any simplification. As it has been noted in Section 4.2, the steady case using a depolymerization flux defined as in (4.1) is not leading to proper results. Therefore it is likely that the unsteady case will also fail to deliver an adequate solution.

As expected by the bad results shown in the previous section, this scheme does not converge: the computed velocities increase to very large numbers as the time advances and a steady state is never reached. The stability of the forward Euler scheme is conditioned by the Péclet number and the Courant number. But neither the Péclet nor the Courant number can be the source of this oscillations since they are not large enough to destabilize the system. Therefore, the divergence could be caused by the same issue regarding the fluxes as in the case presented in Section 4.2.

4.4 Discrepancies in the $V(F, B)$ dependency for the steady case

Most of the numerical simulations are showing a strong disagreement with the theoretical results, meaning that the implementation of the numerical discretization could be incorrect. Still, it can be shown how the numerical results in Section 4.1 can be explained in terms of the theoretical results, thus proving that the implementation of the numerical model is correct. In the following sections, the source of the differences between theoretical and numerical results will be discussed.

To understand the differences between the theoretical and the computed velocity profiles shown in Figure 4.3, it is essential to recall how the velocity profile is obtained analytically, as opposed to how the code computes it.

As explained in Section 2.7, the $V(F, B)$ dependency is obtained by evaluating the amount of $a(x)$ at the leading edge:

$$V = k_{on}\delta exp\left(\frac{-F\delta}{k_B T B}\right)a(x = 0). \tag{4.2}$$

The analytic expression of $a(x = 0)$ is written in terms of J_p:

$$V = k_{on}\delta\frac{k_{-3}}{k_3 + k_{-3}}exp\left(\frac{-F\delta}{k_BTB}\right)\left(A - \frac{J_p\tau}{L}\right), \tag{4.3}$$

and then substituting J_p by its definition in (2.38):

$$J_p = \frac{VB}{\delta\eta}, \tag{4.4}$$

leading to the following expression:

$$V = k_{on}\delta\frac{k_{-3}}{k_3 + k_{-3}}exp\left(\frac{-F\delta}{k_BTB}\right)\left(A - \frac{VB\tau}{\delta\eta L}\right). \tag{4.5}$$

Therefore, the variable J_p is what it is determining the final dependency. Its definition requires to send the right hand side term depending on V to the left hand side in order to obtain the final $V(F, B)$ dependency:

$$V = \frac{\bar{V}}{\kappa\text{exp(w/B)} + \alpha B}, \tag{4.6}$$

here written in terms of parameters that have already been defined in Chapter 2.

On the other hand, the code used to obtain the numerical results presented at Section 4.1, where J_d is taken as a constant, is not computing the polymerization flux J_p as in (4.4). Instead, the condition that is being imposed is the one where the fluxes balance as:

$$J_p = J_dL. \tag{4.7}$$

Working with the analytic solution, if the definition of J_p in (4.4) is not imposed anywhere, the $V(F, B)$ dependency is found to be similar to the one obtained by the numerical simulations. The comparison of $V(F, B)$ between the analytic solution where conditions (4.4) and (4.7) are imposed, the analytic solution where just (4.7) is imposed, and the numerical solution is presented in Figure 4.6. It can be seen how the analytic solution where just (4.7) is imposed shows how the velocity increases with the number of barbed ends B. The rate of this velocity increase is reduced as the B increases. The numerical results show the same behaviour but the values for the velocity are slightly larger.

From the results in Figure 4.6 it can be noted that although the profiles for the velocity when the definition of J_p in (4.4) is imposed to when its not are very different,

they share a common solution for $B = 96\,\mu m^{-1}$. Since the first simulations where computed for $B = 100\,\mu m^{-1}$, a point close to the common solution, the concentration profiles that were being obtained appeared to match the profiles predicted by the theoretical model. It was not until the simulations were computed for values of B away from the common solution that the discrepancies that arise from not imposing (4.4) where appreciated.

Table 4.4 presents the comparison between the protrusion velocity values for $B = 100\,\mu m^{-1}$ and $F = 100\,p\mathrm{N}/\mu m$ obtained numerically, and by the two analytic solutions that can be derived from the same model by imposing different conditions regarding the fluxes. It can be appreciated how the computed value of the protrusion velocity presents a 4% error when compared to the analytic solution obtained by just imposing (4.7).

Therefore, the numerical results can be explained in terms of the theoretical model: if J_p is computed as a constant that balances with J_d, the analytic dependency obtained through approximations can be obtained in a numerical framework where the convective terms are included. The inclusion of the convective terms may be the reason why the numerical result is still presenting a 4% error with the analytic solution that just imposes balance of fluxes. This reasoning comes from observing the behaviour of the computed and analytic solution just imposing balance of fluxes shown in Figure 4.6. The computed results match the analytic curve when the velocity is small. As the number of barbed ends increases and the cell moves faster, the differences between results become more apparent. Since the convective terms are proportional to the protrusion velocity, the differences between the computed results and the analytic results should increase with the velocity.

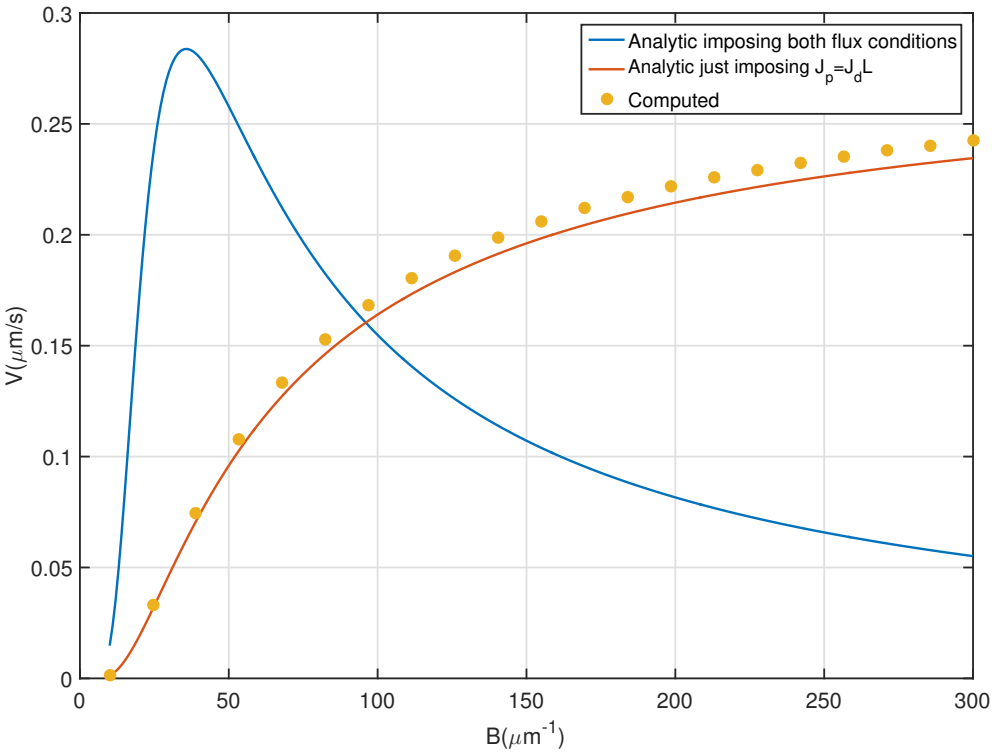

Figure 4.6: Comparison between the computed and analytic protrusion velocity with respect to the number of barbed ends for $F = 100\,p\mathrm{N}/\mu m$. The analytic expressions are the ones obtained when both the condition $J_p = \frac{VB}{\delta\eta}$ and the balance of fluxes are imposed, and when only the balance of fluxes is imposed.

	Computed	Analytic imposing (4.4) and (4.7)	Analytic imposing just (4.7)
Front velocity V	0.1708	0.1548	0.1640

Table 4.3: Computed value of the front velocity compared to the analytic values when different conditions regarding the fluxes are imposed.

It has been established that the code computes a solution that can be obtained from the theoretical model by not imposing the definition in (4.4). The results from the densitites for the F-actin variables and concentrations for the G-actin monomers have been plotted in Figure 4.7 and Figure 4.8. The comparison of the numerical results is being done against the analytic solution that just imposes balance of fluxes. It can be appreciated how the differences are reduced between the computed and the analytic results that are being considered currently. This is due to the fact that the differences in the computed velocity has been reduced to a 4%, reducing the differences in the other variables, since the system is coupled.

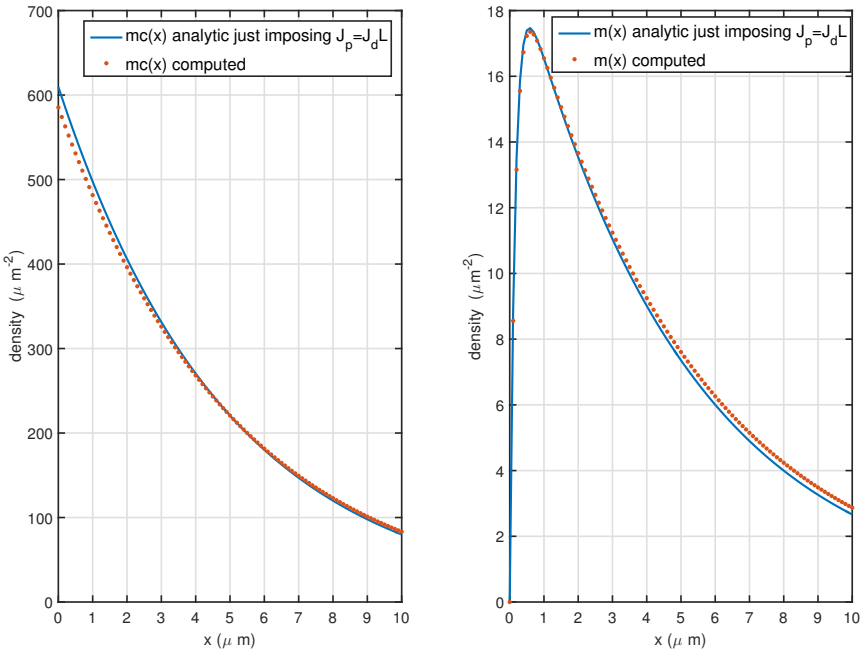

Figure 4.7: Computed densities along the lamellipodium of the pointed ends, both capped and uncapped, compared to the analytic expressions derived from the model just imposing balance of fluxes for $B = 100\,\mu m^{-1}$, $F = 100\,p\mathrm{N}/\mu m$ and $J_d = 7\,\mu M s^{-1}$.

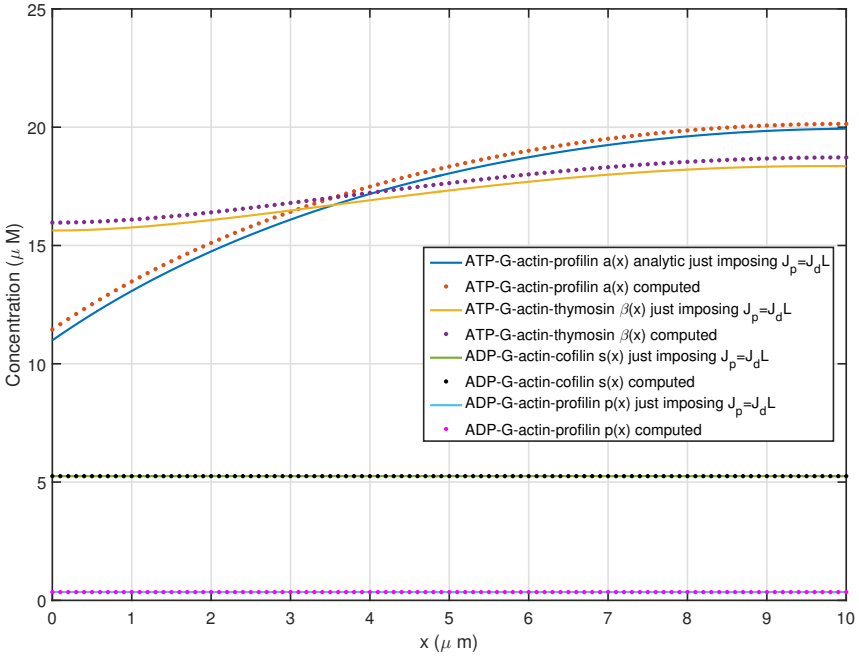

Figure 4.8: Computed concentrations along the lamellipodium of the G-actin monomers compared to the analytic expressions derived from the model just imposing balance of fluxes for $B = 100\,\mu m^{-1}$, $F = 100\,p\mathrm{N}/\mu m$ and $J_d = 7\,\mu M s^{-1}$.

4.5 Issues with the fluxes

The source of discrepancies between the numerical solution and the analytic solution that is obtained by imposing (4.4) and (4.7) for the steady case taking J_d as a constant has been determined. The code used to compute the numerical simulations does not compute J_p imposing (4.4). Instead the polymerization flux is being computed by just imposing balance of fluxes, which is a condition that should be satisfied in order to make the system physically consistent.

The most straightforward way to ensure that both conditions are being imposed would be by computing the polymerization flux as in (4.4), and then compute the depolymerization flux as:

$$J_d = \frac{J_p}{L} = \frac{1}{L}\frac{VB}{\delta\eta}. \tag{4.8}$$

The front velocity obtained from the simulation imposing (4.4) and (4.8) has a value of $V = 8.94\,\mu m\,s^{-1}$, an order of magnitude larger than expected by the theoretical model. This result also leads to density and concentration profiles that do not behave as expected. This seems to indicate that there is some sort of discrepancy between the two conditions that need to be imposed regarding the fluxes.

In the case in which J_d is written in terms of the density of pointed ends $m(x)$, the fact that the fluxes may not be well defined can be seen through the theoretical expressions. The value of the polymerization flux computed using (4.4) for $B = 100\,\mu m^{-1}$ is:

$$J_p = \frac{VB}{\delta\eta} = 70.33\,\mu M\mu m s^{-1}, \tag{4.9}$$

whereas if the polymerization flux is computed as the balance of the depolymerization flux written in terms of the density of pointed ends obtained in (2.8) is:

$$J_p = \int_0^L J_d(x)dx = \int_0^L \frac{V_{dep}}{\delta\eta} m(x)dx = \int_0^L \frac{V_{dep}}{\delta\eta}\frac{n}{V}\frac{t_2}{t_1}\Big[e^{-\frac{x}{Vt_1}} - e^{-\frac{x}{Vt_2}}\Big]dx = \tag{4.10}$$
$$= 38.66\,\mu M\mu m s^{-1}$$

Therefore, the two conditions are not leading to the same value. This could be the reason why both the steady case for $J_d = J_d(m(x))$ and unsteady simulations are not reaching proper results.

4.6 Obtaining the expected $V(F, B)$ dependency

The numerical simulations have only been able to reproduce the theoretical results for the densities and concentrations for $B = 100\mu m$, taking J_d as a constant and computing J_p by imposing balance of the fluxes.

Several tests performed with the code show that the computed value of V is tied to the value that is given to J_d at the beginning of the simulation. In [6], where the one-dimensional model is presented, it fails to mention if the value $J_d = 7\mu M s^{-1}$ is valid for all values of B, but no other value is given.

One of the authors of the model has a paper published in which finite element numerical simulations are performed in order to obtain a two-dimensional model of cell crawling [8]. While the numerical model presented in [8] is much more complex, it includes a description of the actin transport based on the model that has been presented in Chapter 2. For simplicity, the reactions for the G-actin monomers $s(x, t)$ and $p(x, t)$ are omitted.

In the one-dimensional model presented in Chapter 2, the source of depolymerization only appears in the equation describing the G-actin monomer $s(x, t)$. Since the two-dimensional model ignores the equation for $s(x, t)$, the depolymerization source is included in the equation for the G-actin monomer $a(x, t)$. The source is written in terms of an F-actin density variable that represents the density of barbed ends. Since this two-dimensional model ties the depolymerization source to the number of barbed ends. Therefore, the code could be used to find a dependency of J_d on B and F so that the expected $V(F, B)$ dependency is obtained.

To do so, the depolymerization flux has been tuned for each value of B so that the computed value of V is similar to the theoretical value. The dependency that J_d should have on B is shown in Figure 4.9 for $F = 100\, pN/\mu m$.

With that dependency, the computed values of the velocity fit the theoretical curve, as shown in Figure 4.10. It needs to be noted that the values for the flux that have been chosen in order to get the expected dependency are just a rough approximation. The values of the computed velocity should not fit the analytic curve due to the inclusion of convective terms in the system that is being solved numerically. It has already been pointed out that the inclusion of convective terms leads to higher computed values for the velocity.

It needs to be noted that at no point the condition stating that $J_p = \frac{VB}{\delta\eta}$ is not being applied. As stated previously, the only constrain imposed in the polymerization flux is that it must balance the depolymerization flux.

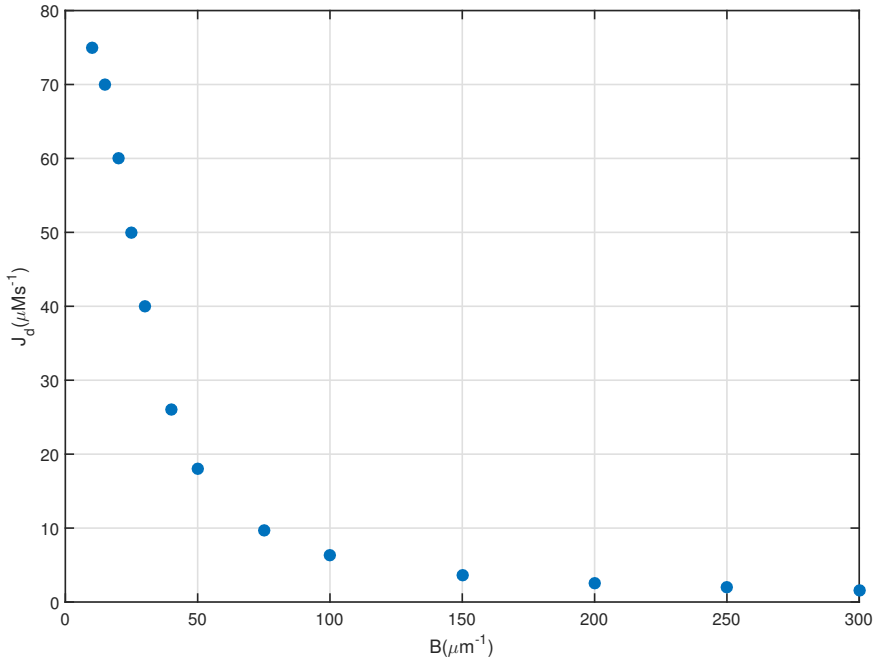

Figure 4.9: Computed values of the depolymerization flux J_d in terms of the number of barbed ends.

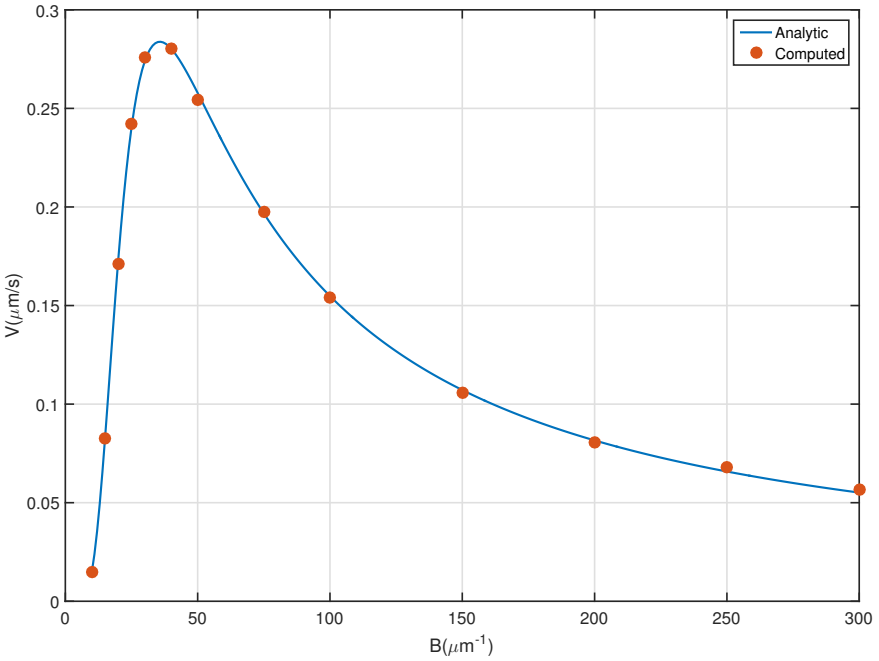

Figure 4.10: Computed front velocity values using the depolymerization flux dependency obtained in Figure 4.9

Chapter 5

Discussion

Understading the actin dynamics occurring in the lamellipodium is essential in order to describe the motility of cells. The recurring assembly and dissassembly of actin from its monomeric form to its filament form is responsible for the protrusion of the lamellipod, the first step of the cell crawling cycle.

The theoretical model that has been studied is described to be an initial attempt to quantify the actin dynamics in protrusion associated with cell motility. A set of nonlinear partial differential equations are solved analytically through approximations and simplifications that decouple the system. On one hand, these simplifications allow the obtention of an analytic solution that characterizes the regulation of acting dynamics in rapidly moving cells. But on the other hand, the range of validity of the model is limited by these simplifications. Numerical simulations are a powerful tool to study the solution of nonlinear systems of equations and to test new hypothesis that lead to systems that cannot be solved analytically.

In this work, the system of partial differential equations that describe the theoretical model has been discretized and several numerical simulations have been performed. The first case that has been considered assumes a time independent system with a depolymerization flux constant along the lampellipodium. The second case also assumes a time independent system, but the depolymerization flux is assumed to be dependant on the variable representing the uncapped pointed ends. Finally, for the third case, the time dependant system using the same depolymerization flux as in the second case. The analytic solution that is presented in the theoretical model has been used to test the validity of the numerical simulations.

For the first case, it has been found that the results from numerical simulations generally agree with the analytic results if the polymerization flux is computed by imposing its balance with the depolymerization flux. There is an small discrepancy that appears due to the inclusion of convective terms in the system that is being

solved numerically. The balance of fluxes is a condition that also gets imposed in the theoretical model, but the polymerization flux is also defined in terms of the protrusion velocity and the number of barbed ends. If this definition for the polymerization flux is imposed in the numerical simulations, the results do not agree with the analytic results predicted by the model. Therefore, although the implemententation of the discretization and linearization of the system is correct, the numerical simulations present an issue between the two conditions regarding the polymerization flux.

For the second and third case, the depolymerization flux is defined in terms of the density of uncapped barbed ends. The theoretical model does not present an analytic solution for this definition of the depolymerization flux. Therefore, the numerical results have been compared to the analytic solution that is obtained when the depolymerization flux is assumed to be a constant. The results for the second case present a great discrepancy with the analytic results. And for the third case, which is the transient version of the second case, the numerical solution has been found to be divergent. In order to find an explanation for these bad results, the polymerization flux has been computed using analytic expressions. It has been found that if the polymerization flux is computed by imposing its definition that depends on the number of barbed ends, its value is different than the one obtained by imposing balance of the fluxes. Therefore, this could be the reason why the numerical simulations lead to results that are not correct.

During the development of this work, a later and much more complex model describing cell motility by the same author was found. In this model where numerical simulations are performed, the depolymerization flux is tied to the variable representing the number of barbed ends. In the theoretical model that has been analyzed in this work, the depolymerization flux is defined as a constant. But it is not specified whether this constant value is valid for any number of barbed ends. Considering that in later models the depolymerization flux has been described in terms of the number of barbed ends, the code has been used as a tool to find a dependency of the depolymerization flux on the number of barbed ends. This dependency allows the numerical simulations to obtain the expected dependency of the protrusion velocity on the number of barbed ends. Still, the imposition of the definition of the polymerization flux is an issue that remains unsolved.

Chapter 6

Conclusions

- The set of nonlinear differential equations describing a theoretical model for actin dynamics in fast moving cells has been discretized using finite elements and linearized using a fixed point iteration.
- The simulations have been run considering a definition of the depolymerization flux to be a constant and a definition to be dependant of the density of uncapped pointed ends. The steady problem has been solved for both types of fluxes. The unsteady problem has been solved for the depolymerization flux written in terms of the density of uncapped barbed ends.
- For the steady problem with a constant depolymerization flux, the numerical results regarding the F-actin densities and G-actin concentrations fit the theoretical model but the computed value of the velocity presents a discrepancy with the analytic value of the velocity. Furthermore, the obtained dependency of the velocity on the number of barbed ends does not fit the analytic dependency predicted by the model
- For the steady problem with a depolymerization flux dependant on the number of barbed ends, the numerical results do not fit the theoretical model and the computed value of the velocity is too large too agree with the proper analytic value.
- The results suggest that the source of the differences between the numerical and analytic results are due to some sort of issue between the conditions that have to be fulfilled by depolymerization and polymerization fluxes.

- The use of numerical simulations is essential in order to analyze cell mechanics, since the equations describing the models cannot be solved analytically without simplifications that may limit the validity of the model.
- The discretization of models of actin treadmilling in a finite element framework can allow the inclusion of more complex phenomena, such as the mechanics of the fluids inside the cell.

Bibliography

[1] National University of Singapore. What steps are involved in lamellipodia assembly. https://www.mechanobio.info/cytoskeleton-dynamics/what-are-lamellipodia-and-lamella/what-steps-are-involved-in-lamellipodia-assembly/.

[2] T. D. Pollard, J. A. Cooper. Actin, a central player in cell shape and movement. *Science*, 326(5957):1208–1212, 2009.

[3] T. D. Pollard, G. G. Borisy. Cellular motility driven by assembly and disassembly of actin filaments. *Cell*, 112(4):453–465, 2003.

[4] D. Raz-Ben Aroush et al. Actin turnover in lamellipodial fragments. *Current Biology*, 27(19):2963–2973, 2017.

[5] D. Pantaloni, C. Le Clainche, M. F. Carlier. Mechanism of actin-based motility. *Science*, 292(5521):1502–1506, 2001.

[6] A. Mogilner, L. Edelstein-Keshet. Regulation of actin dynamics in rapidly moving cells: A quantitative analysis. *Biophysical Journal*, 83(3):1237–1258, 2002.

[7] A. Huerta J. Donea. *Finite Element Methods for Flow Problems*. Wiley, 2003.

[8] B. Rubinstein, K. Jacobson, A. Mogilner. Multiscale two-dimensional modelling of a motile simple-shaped cell. *Multiscale Modeling and Simulation*, 3(2):413–439, 2005.